

# Influence of Architecture, Concentration, and Thermal History on the Poling of Nonlinear Optical Chromophores in Block Copolymer Domains

Melvina Leolukman,<sup>†</sup> Peerasak Paoprasert,<sup>†</sup> Yao Wang,<sup>†</sup> Varun Makhija,<sup>‡</sup> David J. McGee,<sup>‡</sup> and Padma Gopalan<sup>\*,†</sup>

Department of Materials Science and Engineering, University of Wisconsin—Madison, Madison, Wisconsin 53706, and Department of Physics, Drew University, Madison, New Jersey 07940

Received February 12, 2008; Revised Manuscript Received April 26, 2008

**ABSTRACT:** Factors affecting the electric-field-induced poling of nonlinear optical chromophores in block copolymer domains were investigated by encapsulating the chromophores in a linear–diblock copolymer [poly(styrene-*b*-4-vinylpyridine)] and linear–dendritic (poly(methyl methacrylate)–dendron) block copolymer via hydrogen bonding. Temperature-dependent Fourier transform infrared spectroscopy and morphology evaluation by X-ray scattering and transmission electron microscopy were used with in situ second harmonic generation to correlate domain architectures, processing conditions such as thermal history, and chromophore concentrations with poling efficiency. Poling of chromophores encapsulated in the minority domain (spheres or cylinders) of a linear–diblock copolymer was inhibited by the increasing chromophore concentration within the domain and the chemical nature of the majority domain. Chromophore encapsulation in the majority domain produced the most favorable conditions for poling as measured by in situ second harmonic generation. Thermal annealing of the linear–diblock copolymer/chromophore composites resulted in chromophore aggregation with a corresponding decrease in nonlinear optical activity. The linear–dendron/chromophore system presented the most effective architecture for spatially dispersing chromophores. These findings suggest that while well-ordered phase-separated systems such as block copolymers enhance chromophore isolation over homopolymer systems, a more effective approach is to explore polymer chains end functionalized with chromophores.

## Introduction

Spontaneous self-assembly of block copolymers (BCPs) in sub-50 nm domain structures such as spheres, cylinders, and lamellas<sup>1–3</sup> has been used to create templates for pattern transfer<sup>4–7</sup> and also to design new functional materials.<sup>8–10</sup> The control over domain size, shape, and chemistry offers numerous possibilities to tune the properties and define the functionality of the domains. Hence, BCPs offer an ideal test bed to study structure–property relationship in materials with electronic and optical properties. For example, self-assembled rod–coil diblock copolymers exhibit a range of photoluminescence emission based on the morphology formed by the rod–coil diblock copolymers.<sup>11</sup> Block copolymers have also been used to create passive photonic band gap materials, in which the periodic modulation of the dielectric constant produced well-defined optical frequency passbands.<sup>12,13</sup> There are also examples of confining conducting units,<sup>14,15</sup> mesogenic units,<sup>16</sup> or nanoparticles<sup>17</sup> in BCP domains to create functional materials. However, there are very few studies on the confinement of highly dipolar nonlinear optical chromophores in BCP domains to create active nanostructured organic electro-optic (EO) materials.<sup>18–20</sup> In organic EO materials an applied electric field alters the charge distribution in a second-order nonlinear optical chromophore, allowing control of phase, polarization, or speed of a light beam. This can be utilized for applications such as electro-optical modulators, electromagnetic field sensing, and switching devices in optical networks.<sup>21</sup>

Conventional polymeric EO materials are typically guest–host systems, where the guest is a nonlinear optical chromophore and the host is a polymer matrix that primarily provides

mechanical strength to the film. The chromophore is a push–pull molecule with a permanent dipole moment. Application of a dc electric field (i.e., poling field) enables macroscopic EO activity by aligning the dipolar chromophores along the field direction.<sup>21</sup> One of the critical molecular design issues identified from previous studies of EO materials is that the intermolecular electrostatic interactions of high dipole moment chromophores in poled polymers significantly limit the maximum possible macroscopic EO coefficient ( $r_{33}$ ).<sup>22</sup> Possible solutions involve designing new chromophores with more sophisticated shapes that minimize electrostatic interactions.<sup>23–26</sup> An alternate approach is to more fully explore the role of chromophore domains in a polymer matrix and examine how the interface between the two impacts the macroscopic EO activity.

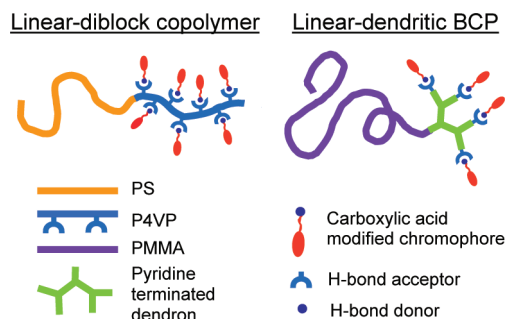
In a study of star-shaped azobenzene chromophores, Gopalan et al.<sup>27</sup> presented morphological evidence for the observed macroscopic activity. When the size of the star-shaped electroactive domains is on average less than 20 nm, the macroscopic EO activity was maximized. As the domain size increases beyond 200 nm, the net EO activity is completely quenched. This provided the motivation to examine the effect of domain size and shape on the EO activity using block copolymer templates. Previous research on hierarchically ordered chromophore arrangements in a crystalline composite of diblock copolymer was reported by Evans et al.<sup>18</sup> where cylindrical and lamellar morphologies with the chromophores arranged within these domains in triclinic symmetry were observed. However, it is not clear whether the chromophores can be poled within the BCP domains as the EO properties of this BCP/chromophore system were not reported. More recently, chromophores covalently bonded to linear–dendritic BCP was reported by Tian et al.<sup>20</sup> where good poling stability and enhancement in EO coefficient were demonstrated. The morphology of these composites was not defined, and the origin of stability of poled order at high temperature in the un-cross-linked system was

\* Corresponding author: Ph (608) 265-4258, Fax (608) 262-8353, e-mail [pgopalan@wisc.edu](mailto:pgopalan@wisc.edu).

<sup>†</sup> University of Wisconsin—Madison.

<sup>‡</sup> Drew University.

**Scheme 1. Schematic of Selective Encapsulation of Nonlinear Optical Chromophores via H-Bonding to a Linear–Diblock and Linear–Dendritic Copolymer**



likewise not clear. Hence, the advantages of controlling the domain size by using a BCP host for EO chromophores are not apparent from these studies.<sup>18,19</sup>

We believe that once selective incorporation of nonlinear optical chromophores in a BCP domain is attained, poling within these domains is considerably more complex than in conventional homopolymer systems. Achieving poled order in confined domains depends on the polymer host architecture, domain size, nature of interaction between the chromophore and polymer host, and concentration of the chromophore within the domains. The tradeoff of course is the possibility to exploit the morphological freedom of BCP systems to create electroactive photonic devices at the nanoscale. In this paper we use block copolymers as a host for selective encapsulation of chromophores and evaluate the effect domain architectures, processing conditions (such as thermal history), and chromophore concentrations have on the poling efficiency. The potential of this study lies in our observations that a synthetically straightforward chromophore encapsulated in a BCP system can exhibit a wide range of second-order nonlinear optical behavior simply as a function of the nanomorphology.

Specifically we investigated two different BCP architectures, namely linear–diblock copolymer and linear–dendritic copolymer. To selectively encapsulate the chromophores within a BCP domain, we utilized noncovalent interactions, such as hydrogen bonding (H-bond). This approach affords (1) flexibility in engineering the chromophore dipole moment independent of the polymer backbone, (2) fine-tuning of desired morphologies by simple variations in the amount of H-bonded chromophores, and (3) confinement of chromophores within the block copolymer domain of specific size and shape. Poly(4-vinylpyridine) (P4VP) is an excellent candidate for one of the blocks of the BCP host due to the ability of the pyridine group to H-bond with carboxylic acid or phenol functionalized chromophores. Poly(styrene-*b*-4-vinylpyridine) [PS-*b*-P4VP] was chosen as the linear–diblock copolymer due to the vast body of literature available on its phase behavior. Linear poly(methyl methacrylate) (PMMA) covalently bound to a dendron with 4VP end groups was chosen as the linear–dendritic analogue (Scheme 1). Factors affecting the selective encapsulation of chromophores in the BCP domains were studied by temperature-dependent Fourier transform infrared spectroscopy (FTIR), while the dynamic evolution of chromophore alignment during poling was monitored in situ via second harmonic generation (SHG) measurements. Morphology was evaluated by X-ray scattering and transmission electron microscopy (TEM).

## Experimental Section

**Materials.** All materials were purchased from Sigma-Aldrich and used without further purification, unless otherwise noted.

**Synthesis of Carboxylic Acid-Modified Thiophene-Based Chromophore (Chr).** The synthetic procedure is shown in Scheme 2. Compounds **1** and **2** were synthesized according to the literature procedures from refs 27 and 28, respectively.

**Synthesis of Compound 3.** 4-Fluorobenzaldehyde (0.90 g, 7.2 mmol), compound **1** (1.90 g, 14.3 mmol), Aliquat-336 (0.02 mL), and potassium carbonate (1.5 g) were dissolved in dimethyl sulfoxide (50 mL). The reaction mixture was heated at 95 °C for 72 h. After cooling to room temperature, the mixture was poured into ice water, extracted with dichloromethane (3 × 50 mL), and the organic layer was washed with water. After solvent removal, the residue was poured into 1 N hydrochloric acid (100 mL) and stirred for 10 min. The aqueous layer was neutralized with sodium carbonate and extracted with dichloromethane (3 × 50 mL). The organic layer was separated, dried over sodium sulfate, and concentrated to yield a brown oil as product (1.5 g, 88%). <sup>1</sup>H NMR (300 MHz, CDCl<sub>3</sub>, δ in ppm): 9.72 (s, 1H), 7.72 (d, *J* = 9 Hz, 2H), 6.68 (d, *J* = 9 Hz, 2H), 3.64 (t, *J* = 6 Hz, 2H), 3.41 (t, *J* = 8 Hz, 2H), 1.86 (s, 1H), 1.59 (m, 4H), 1.39 (m, 4H). <sup>13</sup>C NMR (75 MHz, CDCl<sub>3</sub>, δ in ppm): 190.4, 153.6, 132.3, 124.9, 110.9, 62.7, 52.5, 38.6, 32.7, 27.0, 26.9, 25.8.

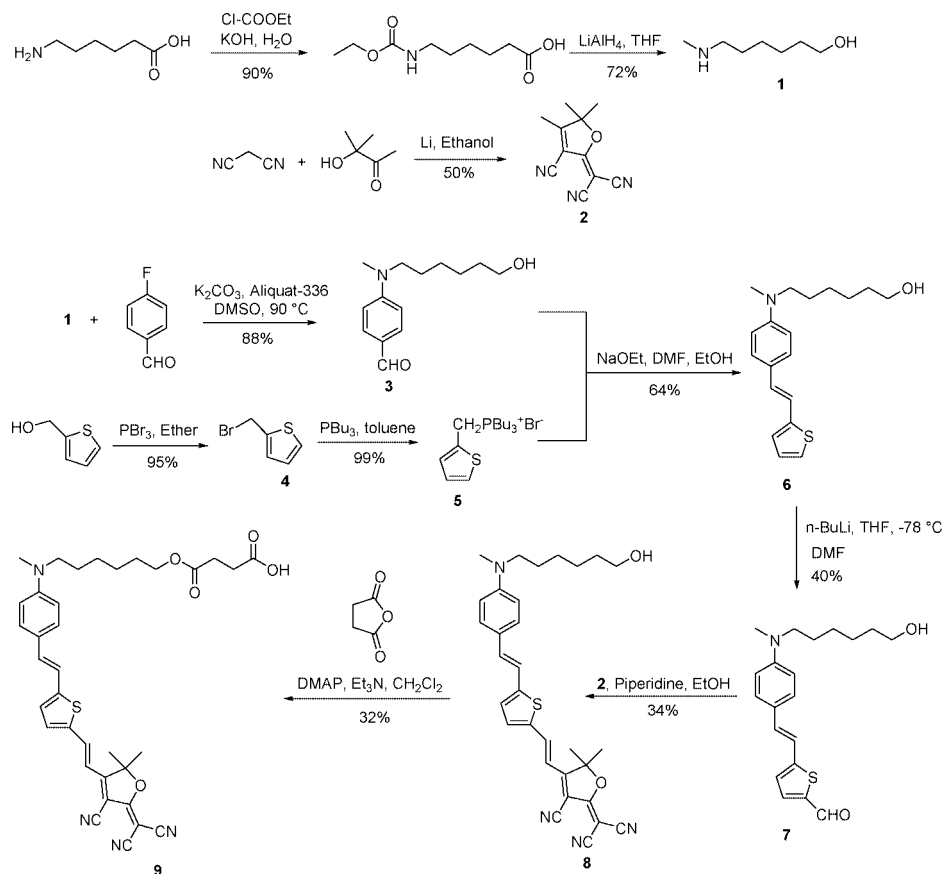
**Synthesis of Compound 4.** 2-Hydroxymethylthiophene (10.0 g, 87.6 mmol) was dissolved in anhydrous diethyl ether (150 mL) at 0 °C in an inert atmosphere. Phosphorous tribromide (11.9 g, 43.8 mmol) was then added dropwise, and the reaction mixture was stirred overnight at room temperature. The reaction mixture was poured into a saturated sodium bicarbonate solution. The organic layer was separated, washed with brine and water, dried over anhydrous sodium sulfate, and concentrated to yield brown liquid (14.8 g, 95%). <sup>1</sup>H NMR (300 MHz, CDCl<sub>3</sub>, δ in ppm): 7.32 (dd, *J* = 5, 1 Hz, 1H), 7.11 (dd, *J* = 5, 1 Hz, 1H), 6.94 (dd, *J* = 5, 4 Hz, 1H), 4.75 (s, 2H). <sup>13</sup>C NMR (75 MHz, CDCl<sub>3</sub>, δ in ppm): 140.7, 128.3, 127.3, 125.6, 27.0.

**Synthesis of Compound 5.** Compound **4** (14.8 g, 83.6 mmol) and tributylphosphine (16.9 g, 83.6 mmol) were added to toluene (100 mL). The reaction mixture was refluxed for 3 days. Toluene was removed from the cooled mixture to yield a white powder (31.4 g, 99%). <sup>1</sup>H NMR (300 MHz, CDCl<sub>3</sub>, δ in ppm): 7.36 (m, 1H), 7.30 (m, 1H), 7.05 (dd, *J* = 6, 4 Hz, 1H), 4.36 (d, *J* = 13 Hz, 2H), 2.47 (m, 6H), 1.52 (m, 12H), 0.97 (t, *J* = 7 Hz, 9H). <sup>13</sup>C NMR (75 MHz, CDCl<sub>3</sub>, δ in ppm): 129.4, 128.2, 127.4, 126.0, 23.6 (d, *J* = 18 Hz), 23.2 (d, *J* = 5 Hz), 21.5 (d, *J* = 48 Hz), 18.3 (d, *J* = 46 Hz), 12.9.

**Synthesis of Compound 6.** Compounds **5** (2.7 g, 7.0 mmol) and **3** (1.5 g, 6.4 mmol) were dissolved in anhydrous *N,N*-dimethylformamide (DMF) (30 mL). Sodium ethoxide (0.60 g, 8.8 mmol) in a small amount of ethanol was added dropwise under nitrogen to the above mixture. The mixture was then heated at 100 °C for 3 days. The reaction was quenched by the addition of water and stirred for 1 h before extracting with diethyl ether (3 × 50 mL). The organic layer was washed with brine and water, dried over sodium sulfate, and purified by column chromatography (dichloromethane:hexane 1:1) to yield an orange solid (1.3 g, 64%). <sup>1</sup>H NMR (300 MHz, CDCl<sub>3</sub>, δ in ppm): 7.37 (d, *J* = 9 Hz, 2H), 7.13 (m, 1H), 7.07 (d, *J* = 16 Hz, 1H), 7.00 (d, *J* = 2 Hz, 1H), 6.99 (d, *J* = 4 Hz, 1H), 6.90 (d, *J* = 16 Hz, 1H), 6.67 (d, *J* = 9 Hz, 2H), 3.62 (t, *J* = 7 Hz, 2H), 3.33 (t, *J* = 9 Hz, 2H), 2.95 (s, 3H), 1.59 (m, 4H), 1.38 (m, 4H). <sup>13</sup>C NMR (75 MHz, CDCl<sub>3</sub>, δ in ppm): 149.1, 144.3, 129.0, 127.8, 127.7, 125.0, 124.6, 123.1, 117.6, 112.2, 63.1, 52.8, 38.6, 33.0, 27.2, 27.0, 25.9.

**Synthesis of Compound 7.** In a three-neck round-bottom flask flushed with nitrogen, compound **6** (1.1 g, 3.5 mmol) was dissolved in anhydrous tetrahydrofuran (30 mL). After the solution was cooled to −78 °C, *n*-butyllithium (2.5 M in hexane) (2.8 mL, 7.0 mmol) was added dropwise. The mixture was then allowed to warm to −20 °C. The mixture was cooled back down to −78 °C, and anhydrous DMF (1.3 mL) was added dropwise. The mixture was slowly warmed to room temperature and stirred overnight. Water (20 mL) was added to quench the reaction, and the mixture was extracted with ethyl ether (3 × 50 mL). The organic layer was washed with water and brine, dried over sodium sulfate, concen-

Scheme 2. Synthesis of Carboxylic Acid-Modified Thiophene-Based Chromophore



trated, and purified by column chromatography (dichloromethane:ethyl acetate 10:1) to yield a brown liquid (0.48 g, 40%).  $^1\text{H}$  NMR (300 MHz,  $\text{CDCl}_3$ ,  $\delta$  in ppm): 9.81 (s, 1H), 7.63 (d,  $J = 4$  Hz, 1H), 7.38 (d,  $J = 9$  Hz, 2H), 7.09 (d,  $J = 16$  Hz, 1H), 7.05 (d,  $J = 4$  Hz, 1H), 6.98 (d,  $J = 16$  Hz, 1H), 6.65 (d,  $J = 9$  Hz, 2H), 3.65 (t,  $J = 6$  Hz, 2H), 3.36 (t,  $J = 8$  Hz, 2H), 2.98 (s, 3H), 1.60 (m, 4H), 1.38 (m, 4H).

**Synthesis of Chromophore 8.** Compounds **2** (0.70 g, 3.5 mmol) and **7** (1.0 g, 2.9 mmol) were dissolved in tetrahydrofuran/ethanol (50 mL, 80:20 by volume). Piperidine (6 drops) was added as catalyst, and the reaction mixture was refluxed overnight. After cooling down, the reaction mixture was concentrated in vacuum and purified by column chromatography (dichloromethane:ethyl acetate 2:1) to yield a dark blue solid as product (0.52 g, 34%).  $^1\text{H}$  NMR (300 MHz,  $\text{CDCl}_3$ ,  $\delta$  in ppm): 7.77 (d,  $J = 16$  Hz, 1H), 7.41 (d,  $J = 9$  Hz, 2H), 7.38 (d,  $J = 4$  Hz, 1H), 7.11 (d,  $J = 16$  Hz, 1H), 7.04 (d,  $J = 4$  Hz, 1H), 7.01 (d,  $J = 15$  Hz, 1H), 6.68 (d,  $J = 9$  Hz, 2H), 6.57 (d,  $J = 15$  Hz, 1H), 3.67 (t,  $J = 6$  Hz, 2H), 3.39 (t,  $J = 7$  Hz, 2H), 3.03 (s, 3H), 1.76 (s, 6H), 1.65–1.35 (m, 8H).  $^{13}\text{C}$  NMR (75 MHz,  $\text{CDCl}_3$ ,  $\delta$  in ppm): 176.0, 173.1, 154.8, 150.3, 139.6, 137.9, 137.5, 135.2, 132.6, 129.1, 127.1, 123.4, 115.8, 112.5, 112.3, 112.0, 111.8, 111.3, 97.1, 96.0, 63.0, 52.6, 38.6, 32.9, 27.3, 27.1, 27.0, 26.7, 25.9. Molecular formula  $\text{C}_{31}\text{H}_{32}\text{N}_4\text{O}_2\text{S}$ . Exact mass + H: calculated 524.7; observed 525.2.

**Synthesis of Chromophore 9.** Chromophore **8** (0.20 g, 0.38 mmol), succinic anhydride (0.076 g, 0.76 mmol), triethylamine (TEA) (0.080 g, 0.76 mmol), and  $N,N$ -(dimethylamino)pyridine (DMAP) (9.3 mg, 0.08 mmol) were dissolved in dichloromethane (20 mL). The mixture was stirred overnight at room temperature and was then washed with brine and water. The organic layer was dried over sodium sulfate and purified by column chromatography (dichloromethane:ethyl acetate 1:2) to yield a blue solid (75 mg, 32%).  $^1\text{H}$  NMR (300 MHz,  $\text{CDCl}_3$ ,  $\delta$  in ppm): 9.79 (s, 1H, OH), 7.77 (d,  $J = 15$  Hz, 1H,  $-\text{CH}=\text{CH}-$ ), 7.40 (d,  $J = 9$  Hz, 2H, ArH), 7.37 (d,  $J = 4$  Hz, 1H, thiophene), 7.10 (d,  $J = 16$  Hz, 1H,  $-\text{CH}=\text{CH}-$ ), 7.04 (d,  $J = 4$  Hz, 1H, thiophene), 7.01 (d,  $J = 16$

Table 1. Summary of the Resulting Morphology of the Composite Due to Increasing Amount of Added Chromophore









PS- <i>b</i> -P4VP $M_n$ (g/mol)	$M_w/M_n$	Chr : 4VP mole ratio	$f_{\text{P4VP-ChrT}}$	Bulk Morphology
35.5	3.6	1 : 17	0.12	P4VP-Chr cylinder
PS	P4VP	1 : 4	0.20	P4VP-Chr cylinder
		1 : 1	0.38	Lamella

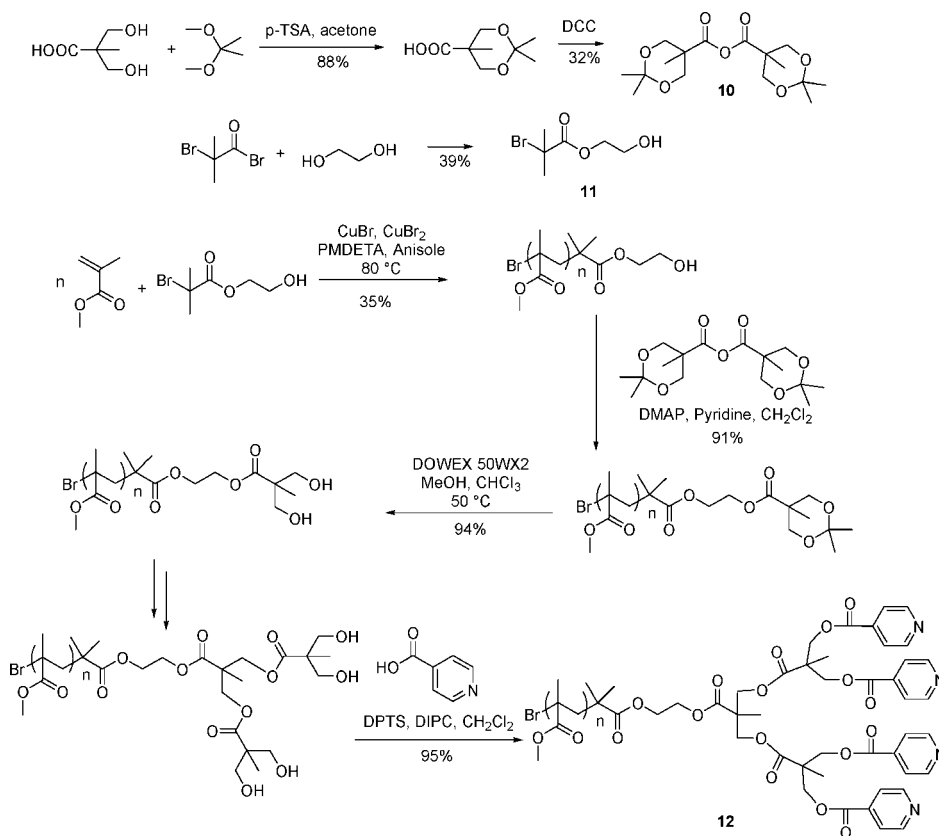
Hz, 1H,  $-\text{CH}=\text{CH}-$ ), 6.68 (d,  $J = 9$  Hz, 2H, thiophene), 6.57 (d,  $J = 15$  Hz, 1H,  $-\text{CH}=\text{CH}-$ ), 4.10 (t,  $J = 7$  Hz, 2H,  $-\text{O}-\text{CH}_2$ ), 3.38 (t,  $J = 8$  Hz, 2H,  $-\text{CH}_2$ ), 3.01 (s, 3H,  $-\text{CH}_3$ ), 2.66 (m, 4H,  $-\text{CH}_2$ ), 1.76 (s, 6H,  $-\text{CH}_3$ ), 1.40–1.20 (m, 8H,  $-\text{CH}_2$ ).  $^{13}\text{C}$  NMR (75 MHz,  $\text{CDCl}_3$ ,  $\delta$  in ppm): 177.4, 176.0, 173.1, 172.4, 154.7, 150.3, 139.6, 137.9, 137.6, 135.1, 129.1, 127.1, 123.5, 115.9, 112.5, 112.1, 111.8, 111.7, 111.3, 97.2, 96.1, 65.0, 56.0, 52.6, 38.6, 29.1, 29.0, 28.7, 27.0, 26.9, 26.7, 26.0. IR (NaCl,  $\nu$ ,  $\text{cm}^{-1}$ ): 3400–3000 (broad), 2964, 2948, 2870, 2239, 1748, 1726, 1611, 1570, 1534, 1448, 1392, 1365, 1290, 1270, 1183, 1120, 1065, 1032, 961, 924. Molecular formula  $\text{C}_{35}\text{H}_{36}\text{N}_4\text{O}_5\text{S}$ . Exact mass – H: calculated 623.8; observed 623.4.  $\lambda_{\text{max}}$  ( $\text{CHCl}_3$ ) 650 nm.

**Synthesis of Diblock Copolymer and Homopolymer.** PS-*b*-P4VP compositions as well as PS and P4VP homopolymers used are summarized in Table 1 and Table 2. PS homopolymer ( $M_n = 92\,300$ ,  $M_w/M_n = 1.08$ ) and PSV2 ( $M_n = 23\,500$ ,  $M_w/M_n = 1.40$ ) were synthesized by living anionic polymerization as previously described,<sup>29–31</sup> while P4VP homopolymer and other PS-*b*-P4VP were purchased from Polymer Source, Inc.

**Synthesis of Linear–Dendritic BCP.** The synthetic scheme for PMMA linear–dendritic BCP is shown in Scheme 3. Acetone–2,2′-bis(hydroxymethyl)propionic anhydride (bis MPA anhydride) (**10**) and atom transfer radical polymerization (ATRP) initiator (**11**) were synthesized according to the literature procedures in refs 32 and 33, respectively.

**Table 2. Summary of the PS-*b*-P4VP Block Copolymer Host Composition, Added Chromophore Concentration, Resulting Morphology, and the Normalized SHG Signal of PS-*b*-P4VP-Chr Composite, Highlighting the Effect of Chromophore Concentration on the Poling Efficiency**

	PS- <i>b</i> -P4VP <i>M<sub>n</sub></i> (g/mol)	<i>M<sub>w</sub></i> / <i>M<sub>n</sub></i>	Chr : 4VP mole ratio	<i>f</i> <sub>P4VP-ChrT</sub>	Bulk Morphology	Normalized SHG (a.u.) Unannealed
P4VP	 9.5 k	1.15	1 : 30	-	-	1.4
PSV1	 3.3 k 18.7 k	1.14	1 : 25	0.88	-	2.0
PSV2	 7.3 k 16.2 k	1.40	1 : 19	0.75	PS cylinder	1.3
PSV2b	 7.3 k 16.2 k 9.5 k	-	1 : 30	0.81	PS cylinder	1.6
PSV3	 20.5 k 36.0 k	1.08	1 : 19	0.70	Lamella	1.0
PSV4	 35.5 k 4.4 k	1.09	1 : 3	0.30	P4VP-Chr cylinder	0
PSV5	 41.1 k 1.9 k	1.07	1 : 1	0.24	Lamella	0
PS	 92.3 k PS	1.08	-	-	-	0

**Scheme 3. Synthesis of PMMA Linear–Dendritic Block Copolymer**

**Synthesis of Hydroxyl-Terminated PMMA by ATRP.** To a 50 mL Schlenk flask, methyl methacrylate (8.0 g, 80 mmol), Cu(I)Br (35.7 mg, 0.25 mmol), Cu(II)Br<sub>2</sub> (2.8 mg, 0.012 mmol), pentamethyldiethylenetriamine (PMDETA) (43 mg, 0.25 mmol), and anisole (5 mL) were charged and degassed three times by freeze–pump–thaw cycles. The ATRP initiator (**11**) (53 mg, 0.25 mmol) was then added, and the mixture was stirred at 80 °C for 90 min. The mixture was precipitated in methanol to yield the hydroxyl-terminated PMMA as a white powder (4.2 g, 35% yield, *M<sub>n</sub>* 18 000, *M<sub>w</sub>*/*M<sub>n</sub>* = 1.11). <sup>1</sup>H NMR (300 MHz, CDCl<sub>3</sub>, δ in ppm): 3.59 (s, –OCH<sub>3</sub>), 1.89–1.80 (m, –CH<sub>2</sub>–, –CH–), 1.02 (s, –CH<sub>3</sub>), 0.84 (s, –CH<sub>3</sub>). <sup>13</sup>C NMR (75 MHz, CDCl<sub>3</sub>, δ in ppm): 178.2, 177.9, 177.1, 54.6, 54.3, 51.9, 45.0, 44.6, 18.8, 16.6. IR (NaCl, ν, cm<sup>–1</sup>): 2990, 2948, 1729, 1480, 1446, 1433, 1383, 1267, 1239, 1190, 1147.




**General Procedure for the Functionalization of Hydroxyl-Terminated PMMA with Acetonide-Protected Bis MPA.** Hydroxyl-terminated PMMA (0.12 mmol) was dissolved in 80 mL of

dichloromethane/pyridine (9:1) solvent mixture. To this solution bis MPA anhydride (**10**) (0.15 g, 0.46 mmol) and DMAP (12.7 mg, 0.10 mmol) were added. The mixture was stirred overnight at room temperature followed by precipitation in methanol to yield the polymer as white powder (91%). <sup>1</sup>H NMR (300 MHz, CDCl<sub>3</sub>, δ in ppm): 3.59 (s, –OCH<sub>3</sub>), 1.89–1.81 (m, –CH<sub>2</sub>–, –CH–), 1.01 (s, –CH<sub>3</sub>), 0.84 (s, –CH<sub>3</sub>). <sup>13</sup>C NMR (75 MHz, CDCl<sub>3</sub>, δ in ppm): 178.2, 177.9, 177.1, 54.6, 54.3, 51.9, 45.1, 44.7, 18.9, 16.6. IR (NaCl, ν, cm<sup>–1</sup>): 2990, 2948, 1729, 1477, 1448, 1433, 1384, 1268, 1239, 1190, 1148.

**General Procedure for the Deprotection of the Acetonide Protecting Groups.** Acetonide-protected PMMA (0.11 mmol) and DOWEX 50WX2 (2 teaspoons) were added in 200 mL of chloroform/methanol (1:10) solution. The mixture was allowed to stir at 50 °C for 4 h. The resin was filtered, and the filtrate was concentrated in vacuum. The crude polymer was redissolved in dichloromethane and precipitated in methanol to yield the polymer as a white powder (94%). <sup>1</sup>H NMR (300 MHz, CDCl<sub>3</sub>, δ in ppm):



**Table 3. Summary of the PS-*b*-P4VP Host Composition, Added Chromophore Concentration, Peak Poling Temperature, Thermal History, and the Resulting Normalized SHG Signal of the Composite Highlighting the Effect of Thermal Annealing**

	PS- <i>b</i> -P4VP <i>M<sub>n</sub></i> (g/mol)	Chr : 4VP mole ratio	Peak temperature (°C)	Normalized SHG (a.u.)	Unannealed (U) / Annealed (A)
PSV1		1 : 25	115	2.0	U
		1 : 25	140-145	0.4	A
PSV2		1 : 19	105-110	1.3	U
		1 : 19	143-145	0.9	A
PSV2b		1 : 30	100-115	1.6	U
		1 : 30	138-142	0.8	A

**Table 4. Summary of the Linear-Dendritic Block Copolymer Composition, Added Chromophore Concentration, Peak Temperature, Thermal History, and the Resulting Normalized SHG Signal**

	Homopolymer <i>M<sub>n</sub></i> (g/mol)	Chr : 4VP mole ratio	Peak temperature (°C)	Normalized SHG (a.u.)	Unannealed (U) / Annealed (A)
PMMA-dendron	20.3 k	1 : 1	82-85	1.6	U
		1 : 1	83	1.2	A

3.60 (s, -OCH<sub>3</sub>), 1.89–1.81 (m, -CH<sub>2</sub>, -CH), 1.02 (s, -CH<sub>3</sub>), 0.85 (s, -CH<sub>3</sub>). IR (NaCl,  $\nu$ , cm<sup>-1</sup>): 2993, 2949, 1733, 1485, 1447, 1435, 1385, 1265, 1239, 1188, 1145.

**Synthesis of PMMA Linear-Dendritic BCP (12).** To 50 mL of dichloromethane the acetonide-deprotected PMMA (0.54 g, 0.03 mmol), (dimethylamino)pyridinium toluene-*p*-sulfonate (DPTS) (93 mg, 0.1 mmol), and isonicotinic acid (24 mg, 0.20 mmol) were added and stirred for 5 min, followed by the addition of diisopropylcarbodiimide (DIPC) (62 mg, 0.49 mmol). This mixture was allowed to stir overnight at room temperature and then precipitated in methanol to yield the PMMA linear dendrons as white powder (0.51 g, 95%, *M<sub>n</sub>* 18 600, *M<sub>w</sub>*/*M<sub>n</sub>* = 1.09). <sup>1</sup>H NMR (300 MHz, CDCl<sub>3</sub>,  $\delta$  in ppm): 8.81 (d, *J* = 6 Hz, ArH), 7.86 (d, *J* = 6 Hz, ArH), 3.60 (s, -OCH<sub>3</sub>), 1.89–1.81 (m, -CH<sub>2</sub>), 1.02 (s, -CH<sub>3</sub>), 0.85 (s, -CH<sub>3</sub>). <sup>13</sup>C NMR (75 MHz, CDCl<sub>3</sub>,  $\delta$  in ppm): 178.1, 177.8, 176.9, 54.5, 54.3, 52.7, 51.9, 44.9, 44.6, 18.8, 16.5. IR (NaCl,  $\nu$ , cm<sup>-1</sup>): 2990, 2947, 1727, 1483, 1447, 1435, 1382, 1270, 1240, 1189, 1147.

**Complex Preparation.** The BCP/chromophore solution was prepared by dropwise addition of 1 wt % solution of BCP in chloroform to a 1 wt % solution of chromophore in chloroform followed by sonication at 55 °C. The BCP/chromophore solution was kept overnight to ensure H-bond formation. The molar ratio and composition of chromophores to the pyridine groups are shown in Tables 1, 2, and 4.

**Sample Preparation.** The bulk samples were prepared by slow evaporation of BCP and BCP/chromophore from chloroform solution. The film samples were prepared by dissolving the BCP/chromophore in cyclopentanone and then drop-casting on indium-tin oxide (ITO)-coated glass purchased from Delta Technologies, Limited. The profilometry (Alpha-Step 200) measurement of the thin film sample thickness was on the order of a micrometer. Annealed samples were prepared by heating the samples at 80 °C for 24 h in vacuum.

**Characterization.** <sup>1</sup>H (300 MHz) and <sup>13</sup>C (75 MHz) NMR spectra were performed in CDCl<sub>3</sub> on a Hermes Varian MercuryPlus 300. Infrared spectra for synthesis characterization were carried out at Bruker Optics Tensor 27. The temperature-dependent transmission infrared spectroscopy was performed on the Nicolet Magna-IR 860 spectrometer in the range 30–150 °C with a heating and cooling step of 10 °C. Gel permeation chromatography (GPC) measurements of homopolymers and linear-dendritic block copolymer were carried out using Viscotek GPCmax VE-2001, two columns (Varian 5M-POLY-008-27 and Varian 5M-POLY-008-32), and Viscotek Model 302 TDA detectors. Tetrahydrofuran was used as an eluent with 1 mL min<sup>-1</sup> flow rate at 30 °C. Molecular weights are quoted with monodisperse linear polystyrene as standard. GPC measurement of PSV2 was performed on a Viscotek

VE-1122 fitted with two columns (Viscotek Viscogel F 022114 and F 022112) and a Viscotek VE-3580 RI detector. 1-Methyl-2-pyrrolidinone containing 0.1 wt % lithium chloride was used as an eluent with 0.80 mL min<sup>-1</sup> flow rate at 50 °C. Mass spectrometer analysis was performed on Applied Biosystems 3200 Q TRAP mass spectrometer system with Q1 scan type. Differential scanning calorimetry measurements were carried out by a TA Instruments DSC Q1000 with heating and cooling rate of 10 °C min<sup>-1</sup> repeated for three cycles. The glass transition temperature (*T<sub>g</sub>*) was measured from the second cycle.

**Transmission Electron Microscope (TEM).** Bulk samples were embedded in epoxy and cured at 70 °C for 24 h. The embedded samples were then microtomed by a Diatome diamond knife at room temperature into a preset thickness of 70 nm using a Reichert-Jung Ultracut E Microtome. The sections were picked up by TEM grids and stained by iodine vapor for 12 h or RuO<sub>4</sub> for 15 min for linear-diblock and linear-dendritic BCP, respectively, before being viewed with bright field Phillip CM 120 TEM at 80 kV accelerating voltage (Medical School Electron Microscopy Facility, University of Wisconsin-Madison). The mass contrast between stained P4VP and unstained PS or PMMA resulted in P4VP appearing darker than PS or PMMA.

**X-ray Scattering.** Small-angle and wide-angle X-ray scattering (SAXS and WAXS) of bulk samples were performed at beamline 8-ID-E, Advanced Photon Source, Argonne National Laboratory. Only the bulk sample of PSV2 and PSV2b was performed on Rigaku SAXS (Materials Science Center, University of Wisconsin), which is equipped with an MM002+ microfocussing X-ray source operated at 40.5 W with multilayer optics to select Cu K $\alpha$  radiation. Three pinholes collimate the beam over 2.0 m to a diameter of about 0.5 mm at the sample position and 1.4 mm at the detector. A Rigaku multiwire area detector with 1024 wires over the 11.5 cm diameter was used. The sample-detector distance was 2.0 m, yielding an angular resolution of 0.042°. The intensity of the diffraction peaks is a function of the magnitude of the scattering vector,  $q = (4\pi/\lambda) \sin \theta$ , where  $\lambda$  is the X-ray wavelength and  $2\theta$  is the scattering angle. The *d*-spacing was calculated from  $d = 2\pi/q^*$ , with  $q^*$  being the position of the primary diffraction peak.

**Second Harmonic Generation (SHG).** In-situ second harmonic generation was used to monitor poling in the linear-diblock copolymer and linear-dendritic copolymer systems. In our experiments, the 3  $\mu$ m thick sample films were mounted on a heating stage with a corona poling wire suspended 1 cm above the film plane. A pulsed 1064 nm Nd:YAG laser beam was directed through the film at an angle of 45°, and the 532 nm second harmonic was separated out and detected by a photomultiplier and associated integrating electronics. All films were poled at a constant 10  $\mu$ A

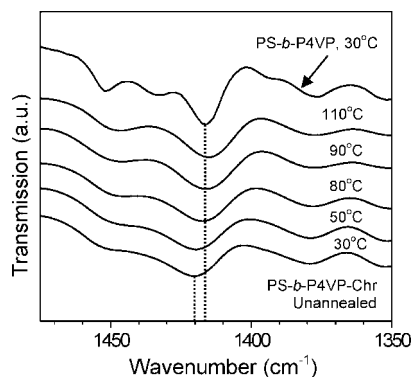


**Figure 1.** Transmission IR spectra of neat PS-*b*-P4VP and temperature-dependent transmission IR spectra of unannealed PS-*b*-P4VP-Chr.

current and a linear heating rate of 5 °C min<sup>-1</sup>. The poling field was maintained as the sample cooled back to room temperature.

Second harmonic generation is typically used to measure the nonlinear optical coefficient  $d_{33}$ , in which case a Maker fringe analysis<sup>34,35</sup> is performed with a quartz reference sample. Since the main focus here is the comparison of BCP films with different morphologies and the identification of factors that impact chromophore poling in BCP domains, the absolute determination of  $d_{33}$  is not necessary. To establish a baseline for comparison with electro-optic polymers commonly reported in the research literature, the SHG signals in Tables 2, 3, and 4 are normalized to a corona poled 3  $\mu$ m thick guest–host blend of 20 wt % Disperse Red 1 (DR1) in amorphous polycarbonate (APC). DR1 is a commercially available nonlinear optical chromophore which has been extensively characterized.<sup>36</sup>

After being poled, different BCP films of the same composition typically exhibited steady-state room temperature SHG signals that varied ~20% from the mean. Fluctuations in poling current caused by surface film defects and variations in film quality may be partially responsible for this, which are the subject of ongoing studies. The maximum SHG signal attained during poling was however consistently reproducible within 5%, and it is the average maximum values that are indicated in Tables 2, 3, and 4 and which are likewise normalized to the maximum SHG observed in the DR1-APC reference sample.

## Results and Discussion

PS-*b*-P4VP is an excellent BCP host due to the ability of the pyridine group to H-bond with carboxylic acid or phenol functionalized chromophores. Various compositions of PS-*b*-P4VP were chosen to investigate the confinement effect on poling efficiency. For a chromophore, we started with a reasonably high dipole moment thiophene-based molecule<sup>37</sup> to allow observable changes in second-order nonlinear optical activity as a function of variation in the BCP composition. We introduced a terminal carboxylic acid group as the H-bonding unit at the alkyl chain headgroup of the chromophore (Scheme 2). The long alkyl chain effectively decouples the dipole of the chromophore from the H-donor group and provides the required conformational flexibility for the chromophore to respond to the dc electric poling field.

The complex formation between the pyridine ring of P4VP and the carboxylic acid of the chromophore was investigated by temperature-dependent FTIR. Upon H-bonding of PS-*b*-P4VP with the chromophore, the 1416 cm<sup>-1</sup> band of neat PS-*b*-P4VP shifted to higher wavenumbers of 1420 cm<sup>-1</sup> due to the changes in the electronic distribution of the pyridine ring (Figure 1), in agreement with previous studies.<sup>38,39</sup> The temperature-dependent transmission IR for unannealed samples showed a shift of the 1420 cm<sup>-1</sup> to lower wavenumbers as the temperature was increased. This shift indicates the breaking of the H-bond in the 50–110 °C temperature range. A similar shift

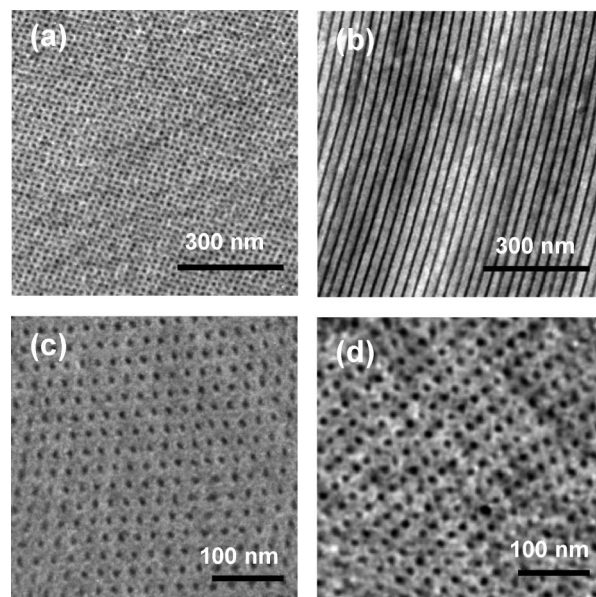


**Figure 2.** TEM images of (a) neat PS-*b*-P4VP, (b) PS-*b*-P4VP-Chr,  $f_{\text{P4VP-Chr}} = 0.38$ , (c) PS-*b*-P4VP-Chr,  $f_{\text{P4VP-Chr}} = 0.20$ , and (d) PS-*b*-P4VP-Chr,  $f_{\text{P4VP-Chr}} = 0.12$ .

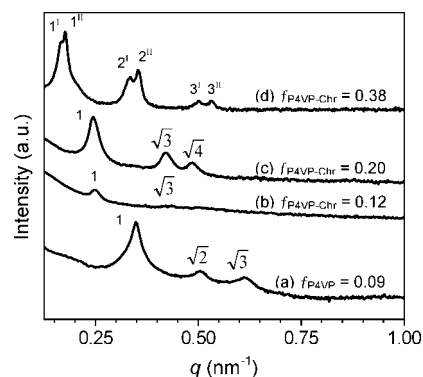


**Figure 3.** SAXS line profiles of (a) PS-*b*-P4VP,  $f_{\text{P4VP}} = 0.09$ , (b) PS-*b*-P4VP-Chr,  $f_{\text{P4VP-Chr}} = 0.12$ , (c) PS-*b*-P4VP-Chr,  $f_{\text{P4VP-Chr}} = 0.20$ , and (d) PS-*b*-P4VP-Chr,  $f_{\text{P4VP-Chr}} = 0.38$ .

was observed in the 50–90 °C temperature range for samples annealed at 80 °C for 24 h. We estimated that less than 5% of these bonds re-form on cooling as calculated from the shift of the pyridine band due to H-bonding. Since the H-bond stability temperature is much lower than the order–disorder transition temperature of the BCP, this strategy allows selective encapsulation of the chromophore in the P4VP domain and releases the chromophores within the P4VP domain when poled above 110 °C. In essence, our approach takes advantage of the control of nanomorphology afforded by the self-assembly of BCP by utilizing noncovalent interactions to selectively encapsulate the chromophores, which is preferable from a poling perspective.

We first discuss results in which a range of morphologies was accessed by simple variation of the amount of chromophore added to the P4VP domain. For the BCP, we utilized a sphere forming PS-*b*-P4VP ( $M_n = 39\,100$  g/mol,  $M_w/M_n = 1.06$ , and P4VP weight fraction of 0.09). The PS-*b*-P4VP phase separated into an array of dark P4VP spheres in a bright PS matrix (Figure 2a). The SAXS scattering peak ratio of 1:√2:√3 implied a body-centered-cubic sphere with  $d$ -spacing of 17.6 nm (Figure 3a). We varied the amount of chromophore added to PS-*b*-P4VP to obtain different size and shape of chromophore domains. The composition and morphologies of PS-*b*-P4VP-chromophores (PS-*b*-P4VP-Chr) are summarized in Table 1. On H-bonding



the chromophore to P4VP with a 1:1 mole ratio, the weight fraction of P4VP-Chr ( $f_{\text{P4VP-Chr}}$ ) is 0.38. The TEM analysis and SAXS scattering peak ratio of 1:2:3 show the formation of lamellar morphology (Figures 2b and 3d), which is in good agreement with what has been reported in the literature regarding PS-*b*-P4VP H-bonded with small molecules.<sup>40,41</sup> A closer examination by SAXS shows that there are two sets of lamella with  $d$ -spacing 35.5 and 37.8 nm ( $q^{\text{I}} = 1^{\text{I}}:2^{\text{I}}:3^{\text{I}}$  and  $q^{\text{II}} = 1^{\text{II}}:2^{\text{II}}:3^{\text{II}}$ , respectively). The higher intensity of  $q^{\text{II}}$  indicates that the majority of lamellar domains have a  $d$ -spacing of 37.8 nm. At present, the origin of the two  $d$ -spacings is unclear and under further investigation. Decreasing the amount of added chromophores ( $f_{\text{P4VP-Chr}} = 0.20$ , Chr:4VP mole ratio of 1:4 and  $f_{\text{P4VP-Chr}} = 0.12$ , Chr:4VP mole ratio of 1:17) led to a hexagonally packed cylindrical morphology (Figure 2c,d) characterized by X-ray scattering peak ratio of  $1:\sqrt{3}:\sqrt{4}$  and  $d$ -spacing of 25.8 and 25.4 nm, respectively (Figure 3b,c).

Although well-defined cylindrical and lamellar morphologies were obtained in the above composites, no detectable SHG signal was observed for these systems. The quenching of SHG can be attributed to the high concentration of the chromophores within the P4VP domain that results in increased electrostatic interactions between the chromophores, which make the poling difficult.

We then varied the chromophore concentration within the P4VP domain by varying the length of the P4VP block and fixing the chromophore amount at 20 wt % with respect to the block copolymer (Table 2). Figure 4 and Figure 5 show the TEM images and X-ray scattering line profiles, respectively. As the ratio of PS to P4VP block length is decreased, the P4VP-Chr domain becomes larger, hence decreasing the chromophore concentration within the P4VP domain. Although the expected spherical morphology ( $f_{\text{P4VP-Chr}} = 0.88$ ) could not be clearly observed in PSV1, the TEM and SAXS results indicate a phase separation with  $d$ -spacing of 12.6 nm ( $q = 0.498 \text{ nm}^{-1}$ ). In PSV2 ( $f_{\text{P4VP-Chr}} = 0.75$ ), hexagonally arranged PS cylinders with a  $d$ -spacing of 28.8 nm ( $q = 0.218 \text{ nm}^{-1}$ ) were observed. The TEM image of PSV4 ( $f_{\text{P4VP-Chr}} = 0.30$ ) demonstrates hexagonally packed P4VP-Chr cylinders. The characteristic lamella scattering peak ratio of 1:2:3 with  $d$ -spacing of 40.3 nm ( $q = 0.156 \text{ nm}^{-1}$ ) observed in PSV4 is attributed to the X-ray beam that was perpendicular to the oriented cylinders long axis direction.<sup>42</sup> PSV5 ( $f_{\text{P4VP-Chr}} = 0.24$ ) showed a lamellar morphology characterized by scattering peak ratio of 1:2:3 and  $d$ -spacing of 32.0 nm ( $q = 0.196 \text{ nm}^{-1}$ ).

The maximum SHG observed during poling of PS-*b*-P4VP-Chr composites of varying compositions are presented in Table 2; as discussed in the Experimental Section, these are normalized to 20 wt % DR1-APC films poled under identical conditions. Typical results for poling a PS-*b*-P4VP-Chr system are shown in Figure 6. As is expected for poled polymer systems, the second harmonic increases from the noise background, rising sharply to its maximum value in the vicinity of 130 °C, and then drops rapidly at higher temperatures. On cooling, the signal again reaches a maximum at 130 °C and continues to maintain some nonzero value at room temperature.

Referring to Table 2, the decrease in P4VP-Chr domain size resulted in increasing chromophore concentration within the P4VP domain, which consequently led to the quenching of the normalized SHG signal from 2.0 (PSV1) to 0 (PSV5). The effect of chromophore concentration within the P4VP domain was investigated further by varying the chromophore concentration in a specific PS-*b*-P4VP system. In the PSV2 system, the chromophore concentration in the P4VP domain was diluted by adding P4VP homopolymer ( $M_n = 9500$ ,  $M_w/M_n = 1.15$ ). The PSV2 blended with P4VP homopolymer (PSV2b) demonstrated a hexagonal cylindrical morphology (Figure 4e) with a

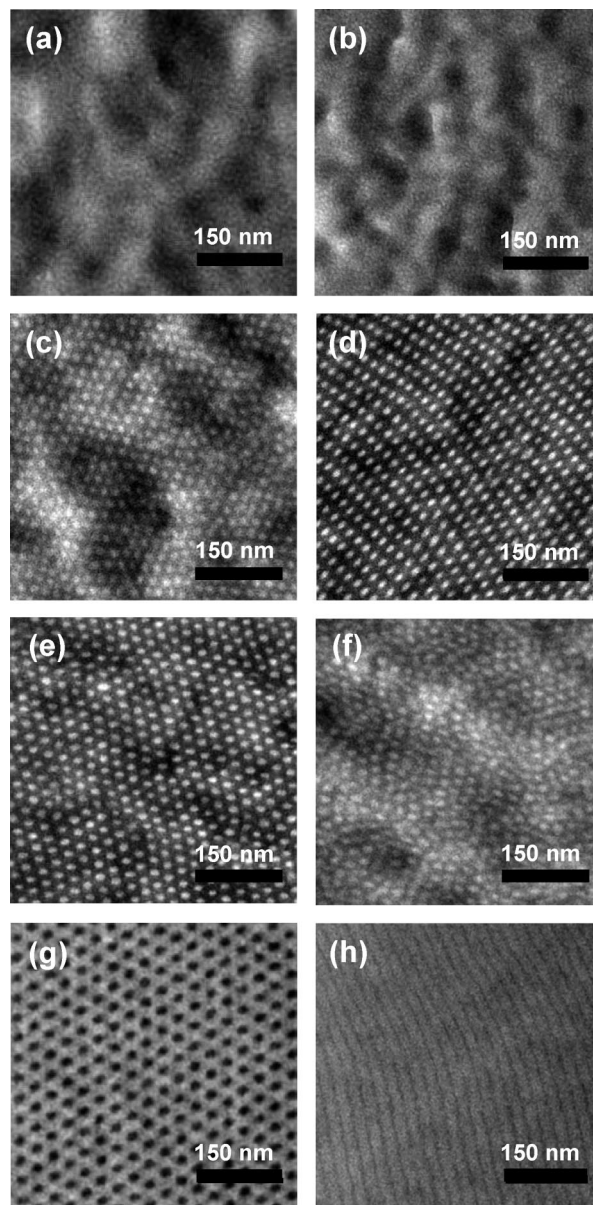


**Figure 4.** TEM images of (a) unannealed and (b) annealed PSV1, (c) unannealed and (d) annealed PSV2, (e) unannealed and (f) annealed PSV2b, (g) unannealed PSV4, and (h) unannealed PSV5.

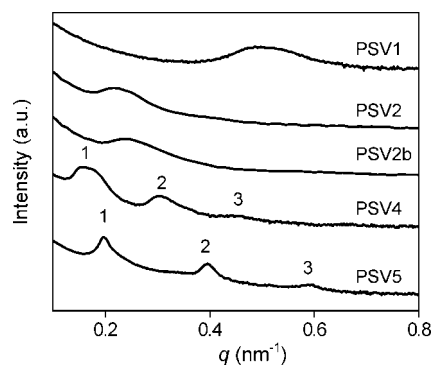


**Figure 5.** SAXS line profiles of PSV1, PSV2, PSV2b, PSV4, and PSV5.

$d$ -spacing of 26.4 nm ( $q = 0.238 \text{ nm}^{-1}$ ). The homopolymer addition led to an increase in the normalized SHG signal from 1.3 to 1.6 for Chr:4VP mole ratio of 1:19 (PSV2) and 1:30 (PSV2b), respectively. These experiments highlight the impor-

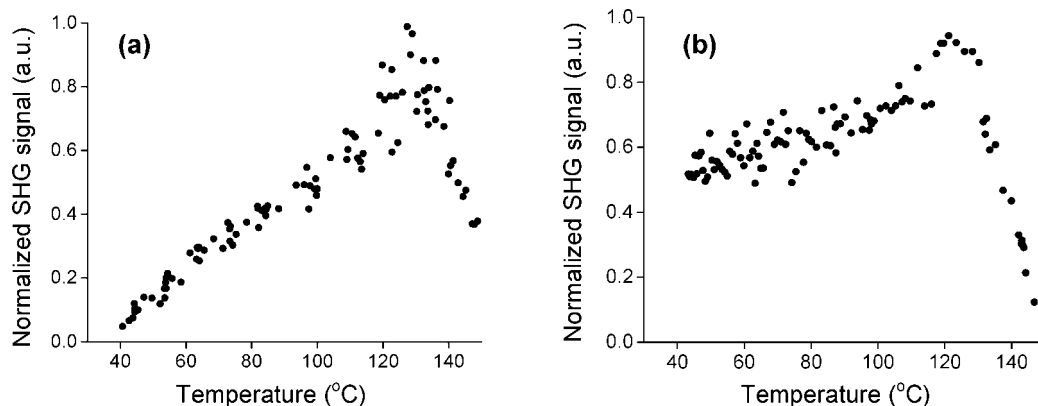


**Figure 6.** Example of in situ second harmonic generation (SHG) signal from PS-*b*-PVP-Chr during (a) heating and (b) cooling. Data shown are from PSV3 in Table 2.

tant fact that the poling efficiency of nonlinear optical chromophores in confined BCP domains depends on the chromophore concentration within the domains.

The data in Table 2 support several interesting observations. The first is the link between the shape of the chromophore domain and the resulting nonlinear optical activity. PSV2 and PSV3 have the same mole ratio of chromophore with respect to P4VP (1:19); however, the normalized SHG of the lamellar morphology PSV3 (1.0) is lower than the cylindrical morphology PSV2 (1.3), which suggests the dependence of electro-optic activity on the shape of the chromophore domain. In addition, the incompatibility of the chromophore with the PS block<sup>43</sup> (resulting in zero SHG from the chromophores in PS host) may also contribute to the decrease in the SHG signal as the PS block length increases. When the concentration of the chromophore in the P4VP domains is high, for example PSV4 and PSV5 with Chr:4VP ratio of 1:1 and 1:3, respectively, the P4VP domains are primarily dominated by the chromophores in both mass and volume. Hence, the P4VP domains are essentially chromophore domains in PS polymer matrix. When the ratio of P4VP block length to PS block length is increased, P4VP becomes a matrix for the chromophore inside the P4VP domains, and the role of PS becomes less significant in the poling process. These results further emphasize the multiple factors affecting the poling of nonlinear optical chromophores in BCP domains, primarily the concentration of the chromophores within the domains as well as the domain shape and the chromophore compatibility with the polymer blocks. Given the range of SHG behavior in Table 2, it is clear that further compositional study of certain morphologies can result in improved poling efficiency over that typically observed in the guest–host system.

It is also of interest to note the temporal stability of chromophore alignment at room temperature. Following removal of the poling field at room temperature, the SHG of the samples in Table 2 was monitored and compared with that of the P4VP homopolymer blended with 20 wt % chromophore. Over a 12 h period, the BCP systems exhibited a 5–7% decrease in SHG compared with an 18% decrease for the homopolymer system. These preliminary results suggest chromophore encapsulation in the BCP domain structure may have an impact on orientational relaxation and are the subject of ongoing investigation.

We then investigated the role of thermal annealing on nonlinear optical activity by annealing PS-*b*-P4VP-Chr at 80 °C for 24 h in vacuum. The annealing temperature is close to the H-bond breaking temperature but lower than the glass transition temperature ( $T_g$ ) of the BCP ( $T_g$  of 116, 130, and 130 °C for PSV1, PSV2, and PSV2b, respectively). Figure 4a–f shows that the morphology of PSV1, PSV2, and PSV2b before and after thermal annealing remains unchanged. Thermal annealing did however result in significant reduction of the nonlinear optical activity as indicated by the

SHG data in Table 3. The more ordered morphology characteristic of annealed samples may enhance electrostatic interaction between chromophores within the domain, leading to increased tendency for antiparallel aggregation. Once the chromophores are aggregated within the domains, it is difficult to deaggregate and align them by the application of dc electric poling field during high-temperature poling, resulting in the observed quenching of SHG (Figure 7).

In a linear–diblock copolymer there are limited options to prevent the chromophores from having interdigitated arrangement within the P4VP domain while maintaining chromophore loading that produces measurable nonlinear optical activity. Hence, we explored a linear–dendritic block copolymer architecture, where it is possible to (1) achieve small chromophore domains by encapsulation in the dendron block, (2) maximize poling via H-bonding of chromophore, and (3) inhibit chromophore aggregation due to the branched nature of the dendron.

Hydroxyl-terminated PMMA homopolymer synthesized by ATRP was end-functionalized with a dendron containing four pyridine units as hydrogen-bond acceptors (Scheme 3). The attachment of the chromophores to the dendron via H-bonding to the four pyridine end groups (Chr:4VP mole ratio of 1:1 or 12.4 wt % loading in the PMMA linear–dendritic block copolymer) resulted in SHG signals comparable to the maximum values seen for the linear–diblock copolymer containing 20 wt % of chromophores (Table 4). Given that the linear–diblock copolymers contain twice the chromophore loading as the PMMA linear–dendritic system, these results strongly suggest that the dendritic architecture is more effective at spatially dispersing the chromophores.

The WAXS line profile is shown in Figure 8 where a scattering peak at 3.16 nm was observed. The 3.16 nm is a good agreement with chromophore length of 3.11 nm predicted by ChemDraw MM2 minimization energy calculation. Schematic representation of the length scales is shown in the inset in Figure 8. The absence of higher order peaks in the X-ray indicates that the linear–dendritic block copolymer primarily acts as a chain end-functionalized with the chromophores in a branched architecture, resulting in efficient dispersion of the chromophores and hence enhanced nonlinear optical activity. The small chromophore domains dispersed in the PMMA linear block can be observed as dark spots in the corresponding TEM image shown in Figure 9. As the chromophores are well dispersed by the dendritic architecture, thermal annealing did not lead to significant quenching of the SHG (Table 4) unlike the linear–diblock copolymer system (Table 3). These findings suggest that while well-ordered phase-separated systems such as block copolymers enhance chromophore isolation over homopolymer systems, a more effective approach is to explore polymer chains end functionalized with chromophores.



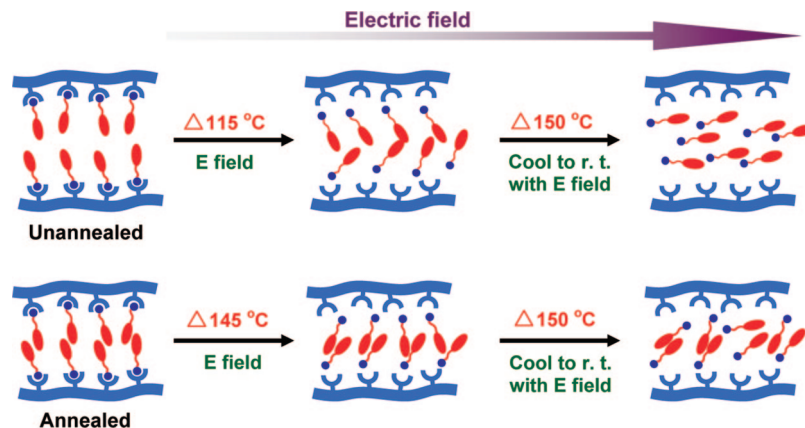


**Figure 7.** Schematic of the poling of chromophores (red ovals) in P4VP domains (blue chain) of unannealed and annealed composites in two steps, first involving heating of the sample above the H-bond stability temperature in the presence of E-field, resulting in release of chromophores within the domain while simultaneously being aligned in the field direction and the second step where aligned dipoles are frozen in space by cooling in the presence of field.

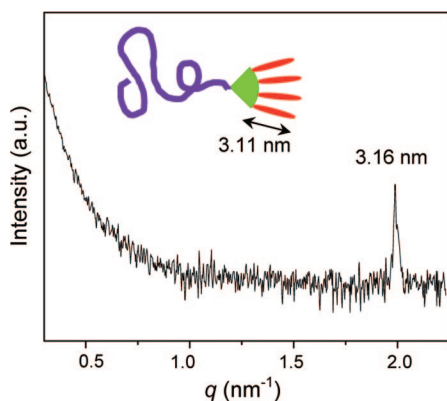


**Figure 8.** WAXS line profile of PMMA linear-dendritic BCP.

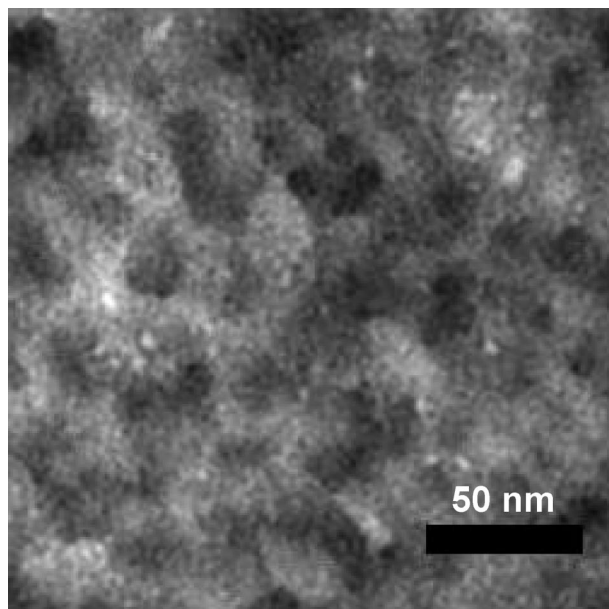


**Figure 9.** TEM image of PMMA linear-dendritic BCP, showing the small chromophore domains (dark spots) dispersed in the PMMA linear block (bright region).

## Conclusion

Nonlinear optical chromophores were selectively encapsulated in a series of linear-diblock and linear-dendritic BCP architectures. Electric field induced poling of the chromophores

within BCP domains led to macroscopic nonlinear optical activity that varied with the domain architecture, processing conditions, and chromophore concentration. The poling efficiency was found to be highly dependent upon the dispersion of the chromophore within the domain, which could be tailored to some extent by controlling the chromophore concentration. Poling of chromophores encapsulated in the minority domain (spheres or cylinders) of a linear-diblock copolymer was inhibited by the increased chromophore concentration within the domain and the chemical nature of the majority domain. Encapsulation of chromophores in the majority domain produced the most favorable conditions for poling. Furthermore, thermal annealing of the linear-diblock copolymer/chromophore composites resulted in chromophore aggregation within the domain, which in turn decreased the SHG signal. Using a different architecture, the linear-dendron/chromophore system provided a relatively straightforward way to control the domain size of chromophores and to maintain their separation within the domains, resulting in improved nonlinear optical properties. These findings identify the critical factors affecting poling of chromophores encapsulated in the phase-separated system. The results of this study not only are applicable to the study of electro-optic polymeric devices but are also important for the broader field of nanostructured photonic materials in which periodic modulation of spatial optical properties is defined via chemical processes. This includes photonic bandgap materials and materials for harmonic frequency generation.

**Acknowledgment.** This work was supported by the NSF-DMR-CAREER 0449688. D.J.M. and V.M. were supported by NSF-DMR 0504105. We also acknowledge the use of Medical School Electron Microscope Facility and Materials Science Center at University of Wisconsin-Madison. The authors acknowledge Dr. Li and Dr. Wang from Argonne National Laboratories for supporting the X-ray diffraction studies.

## References and Notes

- (1) Bates, F. S. *Science* **1991**, *251*, 898–905.
- (2) Bates, F. S.; Fredrickson, G. H. *Annu. Rev. Phys. Chem.* **1990**, *41*, 525–557.
- (3) Bates, F. S.; Fredrickson, G. H. *Phys. Today* **1999**, *52*, 32–38.
- (4) Park, M.; Harrison, C.; Chaikin, P. M.; Register, R. A.; Adamson, D. H. *Science* **1997**, *276*, 1401–1404.
- (5) Segalman, R. A.; Yokoyama, H.; Kramer, E. J. *Adv. Mater.* **2001**, *13*, 1152.
- (6) Shin, K.; Leach, K. A.; Goldbach, J. T.; Kim, D. H.; Jho, J. Y.; Tuominen, M.; Hawker, C. J.; Russell, T. P. *Nano Lett.* **2002**, *2*, 933–936.

- (7) Stoykovich, M. P.; Muller, M.; Kim, S. O.; Solak, H. H.; Edwards, E. W.; de Pablo, J. J.; Nealey, P. F. *Science* **2005**, *308*, 1442–1446.
- (8) Cohen, R. E. *Curr. Opin. Solid State Mater. Sci.* **1999**, *4*, 587.
- (9) Maki-Ontto, R.; de Moel, K.; Polushkin, E.; van Ekenstein, G. A.; ten Brinke, G.; Ikkala, O. *Adv. Mater.* **2002**, *14*, 357–361.
- (10) Ruokolainen, J.; Mäkinen, R.; Torkkeli, M.; Mäkelä, T.; Serimaa, R.; ten Brinke, G.; Ikkala, O. *Science* **1998**, *280*, 557–560.
- (11) Jenekhe, S. A.; Chen, X. L. *Science* **1998**, *279*, 1903–1907.
- (12) Urbas, A.; Fink, Y.; Thomas, E. L. *Macromolecules* **1999**, *32*, 4748–4750.
- (13) Yoon, J.; Mathers, R. T.; Coates, G. W.; Thomas, E. L. *Macromolecules* **2006**, *39*, 1913–1919.
- (14) Cho, G. J.; Park, K. P.; Jang, J. K.; Jung, S. G.; Moon, J.; Kim, T. *Electrochem. Commun.* **2002**, *4*, 336–339.
- (15) Tiitu, M.; Torkkeli, M.; Serimaa, R.; Mäkelä, T.; Ikkala, O. *Solid State Ionics* **2005**, *176*, 1291–1299.
- (16) Kato, T.; Mizoshita, N.; Kishimoto, K. *Angew. Chem., Int. Ed.* **2006**, *45*, 38–68.
- (17) Grubbs, R. B. *J. Polym. Sci., Part A: Polym. Chem.* **2005**, *43*, 4323–4336.
- (18) Evans, C. C.; Bates, F. S.; Ward, M. D. *Chem. Mater.* **2000**, *12*, 236–249.
- (19) Pan, J.; Chen, M. F.; Warner, W.; He, M. Q.; Dalton, L.; Hogen-Esch, T. E. *Macromolecules* **2000**, *33*, 4673–4681.
- (20) Tian, Y. Q.; Chen, C. Y.; Haller, M. A.; Tucker, N. M.; Ka, J. W.; Luo, J. D.; Huang, S.; Jen, A. K. Y. *Macromolecules* **2007**, *40*, 97–104.
- (21) Dalton, L. *Polym. Photonics Appl. I* **2002**, *158*, 1–86.
- (22) Dalton, L. R.; Harper, A. W.; Robinson, B. H. *Proc. Natl. Acad. Sci. U.S.A.* **1997**, *94*, 4842–4847.
- (23) Kang, H.; Facchetti, A.; Jiang, H.; Cariati, E.; Righetto, S.; Ugo, R.; Zuccaccia, C.; Macchioni, A.; Stern, C. L.; Liu, Z. F.; Ho, S. T.; Brown, E. C.; Ratner, M. A.; Marks, T. J. *J. Am. Chem. Soc.* **2007**, *129*, 3267–3286.
- (24) Kim, T. D.; Kang, J. W.; Luo, J. D.; Jang, S. H.; Ka, J. W.; Tucker, N.; Benedict, J. B.; Dalton, L. R.; Gray, T.; Overney, R. M.; Park, D. H.; Herman, W. N.; Jen, A. K. Y. *J. Am. Chem. Soc.* **2007**, *129*, 488–489.
- (25) Kim, T. D.; Luo, J. D.; Ka, J. W.; Hau, S.; Tian, Y. Q.; Shi, Z. W.; Tucker, N. M.; Jang, S. H.; Kang, J. W.; Jen, A. K. Y. *Adv. Mater.* **2006**, *18*, 3038.
- (26) Luo, J. D.; Huang, S.; Cheng, Y. J.; Kim, T. D.; Shi, Z. W.; Zhou, X. H.; Jen, A. K. Y. *Org. Lett.* **2007**, *9*, 4471–4474.
- (27) Gopalan, P.; Katz, H. E.; McGee, D. J.; Erben, C.; Zielinski, T.; Bousquet, D.; Muller, D.; Grazul, J.; Olsson, Y. *J. Am. Chem. Soc.* **2004**, *126*, 1741–1747.
- (28) Lazny, R.; Nodzevska, A.; Wolosewicz, K. *Synthesis* **2003**, 2858–2864.
- (29) Lee, K. M.; Han, C. D. *Macromolecules* **2002**, *35*, 760–769.
- (30) Mao, G. P.; Wang, J. G.; Clingman, S. R.; Ober, C. K.; Chen, J. T.; Thomas, E. L. *Macromolecules* **1997**, *30*, 2556–2567.
- (31) Gao, Z.; Varshney, S. K.; Wong, S.; Eisenberg, A. *Macromolecules* **1994**, *27*, 7923–7927.
- (32) Magbitang, T.; Lee, V. Y.; Cha, J. N.; Wang, H. L.; Chung, W. R.; Miller, R. D.; Dubois, G.; Volksen, W.; Kim, H. C.; Hedrick, J. L. *Angew. Chem., Int. Ed.* **2005**, *44*, 7574–7580.
- (33) White, M. A.; Johnson, J. A.; Koberstein, J. T.; Turro, N. J. *J. Am. Chem. Soc.* **2006**, *128*, 11356–11357.
- (34) Herman, W. N.; Hayden, L. M. *J. Opt. Soc. Am. B* **1995**, *12*, 416–427.
- (35) Jerphagn, J.; Kurtz, S. K. *J. Appl. Phys.* **1970**, *41*, 1667.
- (36) Hagen, J. A.; Grote, J. G.; Zetts, J. S.; Diggs, D. E.; Nelson, R. L.; Hopkins, F. K.; Yaney, P. P.; Jen, A. K.; Dalton, L. R. *Proc. SPIE* **2005**, *5724*, 217–223.
- (37) Shi, Y. Q.; Zhang, C.; Zhang, H.; Bechtel, J. H.; Dalton, L. R.; Robinson, B. H.; Steier, W. H. *Science* **2000**, *288*, 119–122.
- (38) Lee, J. Y.; Painter, P. C.; Coleman, M. M. *Macromolecules* **1988**, *21*, 954–960.
- (39) Ruokolainen, J.; tenBrinke, G.; Ikkala, O.; Torkkeli, M.; Serimaa, R. *Macromolecules* **1996**, *29*, 3409–3415.
- (40) Ruokolainen, J.; Saariaho, M.; Ikkala, O.; ten Brinke, G.; Thomas, E. L.; Torkkeli, M.; Serimaa, R. *Macromolecules* **1999**, *32*, 1152–1158.
- (41) Ruokolainen, J.; ten Brinke, G.; Ikkala, O. *Adv. Mater.* **1999**, *11*, 777–780.
- (42) Hayakawa, T.; Wang, J. G.; Sundararajan, N.; Xiang, M. L.; Li, X. F.; Glusen, B.; Leung, G. C.; Ueda, M.; Ober, C. K. *J. Phys. Org. Chem.* **2000**, *13*, 787–795.
- (43) Banach, M. J.; Alexander, M. D.; Caracci, S.; Vaia, R. A. *Chem. Mater.* **1999**, *11*, 2554–2561.

MA800318S